Lab on a Chip

Accepted Manuscript

ROYAL SOCIETY OF CHEMISTRY

www.rsc.org/loc

Generating Electric Fields in PDMS Microfluidic Devices with Salt Water Electrodes

Adam Sciambi[a] and Adam R. Abate[*a]

Received (in XXX, XXX) Xth XXXXXXXXX 20XX, Accepted Xth XXXXXXXXX 20XX
DOI: 10.1039/b000000x

Droplet merging and sorting in microfluidic devices usually rely on electric fields generated by solid metal electrodes. We show that simpler and more reliable salt water electrodes, despite their lower conductivity, can perform the same droplet manipulations at the same voltages.

In droplet microfluidics, each droplet serves as a picoliter-volume "test tube," allowing millions of reactions to be run in parallel using little total reagent[1-3]. By flowing reagents through channels, it is possible to generate, split, and sort droplets by size using purely passive manipulations. To perform complex reactions in the droplets, however, active manipulations are needed, such as controllably merging pairs of droplets and sorting droplets based on fluorescence, both of which can be accomplished with electric fields. For droplet merger or reagent addition, localized fields briefly destabilize the droplets, allowing pairs of droplets to coalesce[4-7] or droplets to be injected with reagent (picoinjection)[8]. Electric fields can also be used to direct droplets of a set fluorescence into a collection channel[9-12] or merged into an aqueous stream, where their contents can be accessed[13]. These important active manipulations necessitate methods for fabricating and utilizing electrodes in microfluidic devices.

The most common technique for fabricating electrodes in droplet microfluidic devices is to fill a microfluidic guide channel with molten indium solder that, once cooled, hardens into a solid metal electrode; the electrode can then be energized via electrical contact with a protruding metal pin.[6-14] Solder electrodes are simpler than patterning metal onto a glass substrate to which the microfluidic channels are bound[4,5] because they do not require electrode-channel alignment and also can be fabricated in under an hour with no specialized equipment. They also have more versatility and precision than inserting straight, rigid wires into the PDMS channels.[15] When making solder electrodes, the device is heated to 90°C and low-melting point indium solder is fed into the channel inlet; upon contacting the heated device, the solder becomes molten, displacing the air and filling the guide channel, and yielding an electrode in the shape of the guide channel. This method of fabricating electrodes, while simple, limits the kinds of electrode geometries that can be achieved. For example, because long channels have high hydrodynamic resistance and resist solder flow, and sharp turns trap air bubbles, such geometries are difficult to fabricate. In addition, once solidified, the delicate metal electrodes can tear during thermal contraction or handling of the device, resulting in a disconnected electrode and a device dud.

Here, we present a simple and reliable method for integrating electrodes into droplet-based microfluidic devices. Like solder-based electrodes, we fabricate guide channels in the shape of the electrode we desire on the microfluidic device; the guide channel is then filled with a nearly-saturated 5M NaCl aqueous solution. The salt solution has a much higher resistivity (4.42 Ω·cm) than indium (8.37 μΩ·cm), but as we show, its conductivity is sufficient to carry tens-of-kilohertz, high-voltage signals due to the low characteristic capacitances of microfluidic devices. These small capacitances ensure that the signals are not shunted elsewhere despite passing through resistive electrodes. Recently, we have presented microfluidic workflows that mentioned use of salt water electrodes for droplet merger[16] and picoinjection[16,17], and even demonstrated that a flowing reagent channel can serve as an electrode[18]. Here, for the first time, we describe and thoroughly characterize the salt water electrode and demonstrate its application to common and important droplet-based microfluidic operations.

Liquid metals, which have both the conductivity of solder and are liquid at room temperature like salt solutions, have also been used for electrodes in microfluidic devices[19,20]. One such liquid metal is Galistan, which freezes at -19°C and is by weight 68% Ga, 22% In, and 10% Sn. Non-toxic, Galistan is a good candidate for microfluidic electrodes except that it is difficult to clear from surfaces once smeared, leaving messy, semi-permanent electrical connections in its place. Salt water can easily be cleaned with a paper towel and dries into insulating salt crystals. Liquid metal electrodes also develop a semi-firm skin of surface oxide when exposed to air such that injection into narrow channels is difficult. Because of these issues, as well as the fact that the high conductivity of liquid metals are not necessary based on our analysis, simple to create and readily-available salt water is

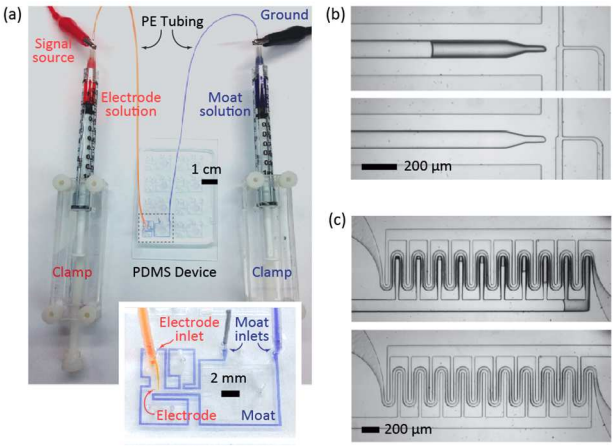

Fig. 1 (a) Photograph of salt water electrode setup, showing pressurized and biased leads inserted into the device (inset). (b) Channel filling with salt water (light gray) and displacing air (dark gray) over 10 s from top image to bottom. (c) Similar filling in a more complicated electrode geometry.

suitable in most cases.

To implement salt water electrodes, syringes are filled with the 5 M NaCl solution and inserted into custom acrylic clamps (Fig 1a.) The acrylic clamps apply a constant pressure to the salt solution via a screw pushing on the syringe plunger. The syringes are connected to the device electrode via a 27 gauge needle and polyethylene tubing. The tubing has an inner diameter of 380 µm for a resistance of 4 kΩ/cm, and alligator clips connected to an exposed section of the syringe needle provide electrical contact. A metal wire inserted into the inlet of a channel pre-filled with salt solution will also work as a lead. The driving bias is generated by a low-cost lamp inverter (Digikey, BXA-12579) when a constant 20 kHz signal up to 1500 V is needed, or by a high-voltage amplifier (Trek, 609E-6) when a higher-frequency signal is required. We often incorporate two electrodes into the device, one for the high-voltage signal (Fig 1a, orange electrode) and one for a ground (Fig 1a, blue electrode). The grounded "moat" channel, seen more clearly in the inset, surrounds both the high-voltage electrode and the other inlets to prevent stray fields from inadvertently merging or otherwise affecting droplets at other locations on the device.

A benefit of the salt water electrode is that, because salt water is liquid at room temperature, it can be introduced into the channel via a pressurized syringe. When coupled with the gas permeability of PDMS devices[21], this enables simple electrode filling and the fabrication of electrodes lacking flow outlets – geometries difficult to achieve with molten solder techniques. The pressurized salt water forces the air initially in the electrode channel into the surrounding PDMS walls, resulting in a fully-filled, air-free electrode. The filling of an electrode with this method is depicted in the progression shown in Figs. 1b and 1c, seconds later, fully filled (bottom). The rate at which the air is absorbed increases with a larger surface-to-volume ratio, so that narrower channels fill faster, as is evident in Fig. 1c. Care must be taken when filling electrodes this way because, for a few minutes after pressurizing, the displaced air in the PDMS can diffuse back into the electrode channel or into neighbouring PDMS channels that are at a lower pressure. For longer channels, like the moat in Fig. 1a, it is helpful to include a flow outlet so that the air can be displaced rapidly.

An obvious concern for the salt water electrode is that, because the conductivity of salt water is not as high as that of metal, input voltage signals may be attenuated on their way to the other end. Attenuation is a consequence of resistive electrodes being capacitively coupled to the space around them, allowing a signal to preferentially transfer elsewhere instead of travelling down the electrode. The resistive electrode, acting as a low-pass filter, will not affect low-frequency or direct current applications. Nevertheless, higher frequencies often are necessary in droplet-based microfluidic applications, such as for effective droplet merger or high speed sorting.

The well-known cut-off frequency f above which a signal travelling along a line resistance R will be shunted across a capacitance C is $f = 1/2\pi RC$. As an example, a 5M salt water electrode that has a 50 µm square cross section and is 10 mm long has a resistance of 180 kΩ. From the roll-off formula, a 10 kHz signal can be transmitted down this line if the capacitance is less than 88 pF. This capacitance is, in fact, quite large at the scale of most microfluidic devices.

The reason microchannel electrode capacitances are small is that capacitance decreases linearly with capacitor size; hence, small capacitors have small capacitances. For example, the usual

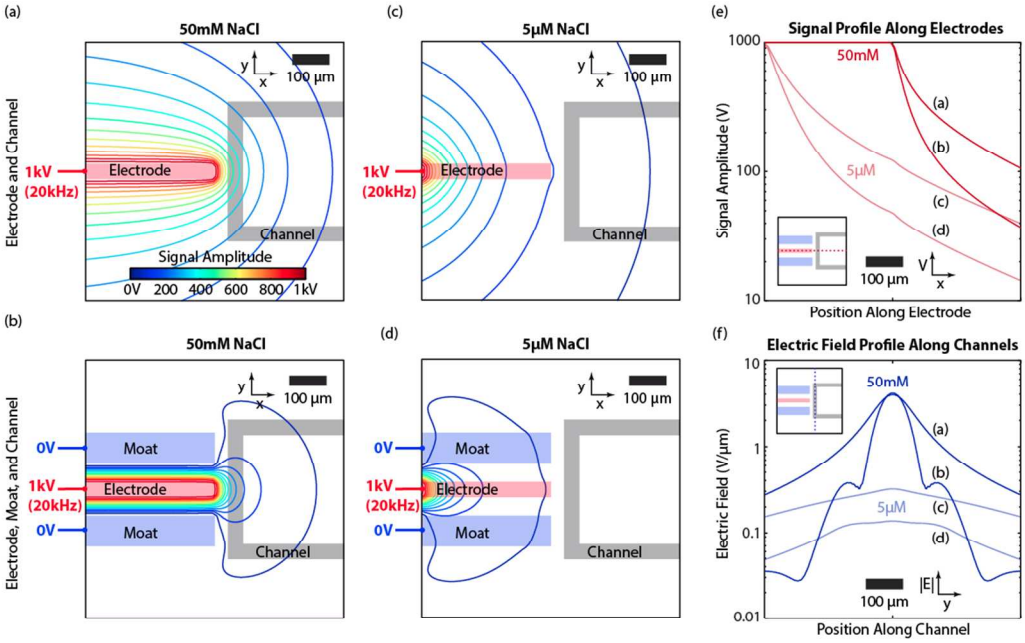

Fig. 2 A 3D simulation of potentials generated by 50 µm tall electrodes for different configurations and salt concentrations. (a) Signal amplitude in the device plane for a 50 mM NaCl electrode with a signal frequency of 20 kHz, and (b) the same with a grounded moat. (c-d) are the same as (a-b) respectively except with a salt concentration of 5 µM. Scale/color bars the same for (a-d). (e) Amplitude profile along the electrode for (a-d), and (f) electric field magnitude along the channel for (a-d).

where each figure shows an electrode in mid fill (top) and ten formula describing the capacitance for *parallel* plates of length *l*,

width w, and separation a is $C_p \approx \epsilon_0 [\,^{lw}/_a]$. If l = 5 mm, w = 1 mm, and a = 10 μm, then C_p = 4.4 pF, which is miniscule: a device with such a capacitance could carry a 10 kHz signal even if its resistance was over 3MΩ. In practice, the capacitances are even smaller due to the two-dimensional nature of these devices; rarely are there geometries that lead to high capacitances like large, closely spaced parallel plates. To make this point, consider two equal, coplanar plates separated by a small gap a, of width w in the direction moving away from the gap, and of length l along the gap. The *coplanar* capacitance C_{cp} in the limit $w/a >> 1$ from eq. (1) in Ref. 22 is $C_{cp} \approx \epsilon_0 \, l \, [^2/_\pi \ln(^{4w}/_a + 2)]$. Two coplanar plates ($l$ = 5 mm, w = 1 mm) and separated by a = 10 μm, have a capacitance of 0.15 pF.

The mutual capacitance between two local conductors is not the only capacitance that might be important. The voltage necessary to charge a lone conductor relative to ground at infinity, known as self-capacitance, can also be significant. The self-capacitance of a thin straight wire of length L and radius r is approximately $C \approx 2\pi\epsilon \, L/\ln(L/r)$.[23] This, however, corresponds to a comparably small 0.22 pF for a 10 mm long, 50 μm diameter conductor.

These calculations are consistent with our simulation of the signal amplitude in the vicinity of a biased salt water electrode in a PDMS device (Fig. 2). The 3D finite-element simulation shows that there is negligible attenuation of the potential along the device both when a 50 mM electrode is unshielded (Fig. 2a) and shielded by a 50 mM moat attached to ground (Fig. 2b). In the latter, the moat serves to limit the signal range outside the electrode without a significant reduction in local electric field near the tip. 50 mM is a hundredth the concentration of saturated salt water, but to see attenuation, much lower salt concentrations are needed. At 5 μM, the signal attenuates rapidly along the electrode, both when unshielded (Fig. 2c) and shielded with a 5 μM moat (Fig. 2d). In Fig. 2c, the signal attenuation originates entirely from the electrode's self-capacitance, whereas the loss in Fig. 2d is from the mutual capacitance between electrode and moat.

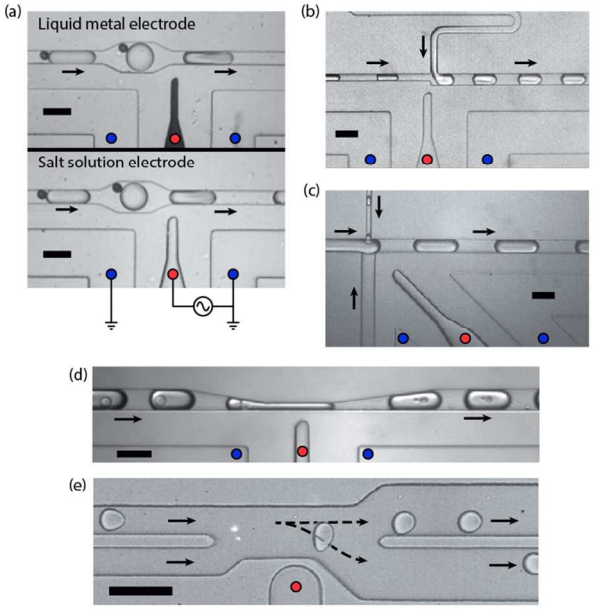

Fig. 3 (a) Comparison of droplet merger devices using a liquid metal electrode (top) and 5 M salt water electrode (bottom). Merger occurs reliably in both for signal amplitudes around 200 V. Salt water electrodes also work well with (b) picoinjection, (c) drop-stream merger, (d) rupture of encapsulated double emulsions, and (e) sorting. Scale bars are 100 μm, arrows indicate fluid flow, and red and blue dot-labeled channels correspond to electrodes and moats, respectively.

A plot of the attenuation along the electrode is given in Fig. 2e with a diagram of the line cut in the inset. Again, the 50 mM electrode has minimal loss of signal down its length while the 5 μM electrode falls to a tenth of its bias at the tip. For interface destabilization and dielectrophoresis, the electric field in the channel is the more relevant quantity and its magnitude is shown in Fig. 2f. As expected, the 5 μM field is much lower in the channel than the 50 mM, and the signal-localizing effect of the moat for 50 mM is lost for 5 μM.

A potential limitation of salt water electrodes is that when high voltages are applied, electrolysis may cause the salt water to vaporize, creating air bubbles that can interrupt current flow. Electrolysis can occur when voltages as low as 2 V are applied across pure water, but it requires a sustained current because build-up of charge at the electrodes rapidly counters the applied voltage. This is a limitation of the salt water electrode: very little current can be carried by it. Fortunately, the breakdown voltage of PDMS, below which it is effectively an insulator, is above 200 V/μm [24] and so electrodes can be spaced to limit leakage current. In the no-leakage-current case for typical devices, we estimate less than a picoliter of gas will be generated for an application of 1 kV DC. To test our electrode's ability to carry a signal, we use a 50 μm square microfluidic channel (180 kΩ/cm) up to 5 cm long and applied at 2 kV signal (peak-to-peak) from near DC to 50 kHz. We observe minimal attenuation along the electrode length and no gas accumulation, illustrating that bubbling due to electrolysis is not significant at the voltages commonly utilized for droplet-based microfluidic applications.

Ultimately, the most telling test of an electrode is how well it performs in practice. To this end, we construct microfluidic devices for performing the most common droplet manipulation techniques that utilize electrodes, and compare their effectiveness to liquid metal electrodes (Fig. 3). We drive all electrodes at 20 kHz with signal amplitudes ranging from 100 V to 1 kV. A direct comparison between two water-in-oil droplet merger devices is shown in Fig. 3a, with the top using a liquid metal electrode and the bottom using a salt water electrode. In both examples, pairs of droplets enter from the left and pass in front of the electrode, where the maximum electric field is applied and merger induced. For these devices, we find that both require a minimum of 200 V signal to achieve perfect merging, and experience inconsistent merging at 180 V. The similar range of effective operation indicates that for this operation, the salt water electrodes perform equivalently to the metal electrodes. Furthermore, the electrodes continue to function well when reduced to 50 mM from 5 M (as in the simulation), though they are less reliable at 5 mM, and both function without change over many hours of continual operation. Three other reagent addition techniques that rely on electrodes are picoinjection (Fig. 3b), merger of a droplet with a forming droplet (Fig. 3c), and rupture of water-oil-water double emulsion encapsulated in aqueous drops[25] (Fig 3d). In all cases, robust

merger is achieved for 100 V signals, demonstrating that these electrodes are effective for these operations too.

Merging droplets with other droplets or with continuous streams is an easy operation for an electrode to perform because in these instances the sinusoidal signal is applied continuously and need not be turned on and off. Hence, the rate at which the signals travel down the electrode is immaterial since this will result only in a phase delay that is of no functional importance. Another droplet microfluidic operation, however, in which the signal must be turned on and off rapidly is dielectrophoretic droplet sorting. To investigate whether salt water electrodes are sufficient for this application, we also test a droplet sorting device (Fig. 3e). In this device, the droplets flow through a focused laser beam (white dot) that excites fluorescent dyes contained within them; if the dye concentration within a given droplet is above a threshold value, a computer and high voltage amplifier output a 50 μs, 1500 V pulse to the electrode. This pulse travels through the salt water electrode and generates an electric field in the microfluidic channel that polarizes the droplet; polarization results in a dielectrophoretic force that attracts the droplet towards the electrode, deflecting it into streamlines that carry it into the collection channel. If the electric field is not applied, the droplet remains in streamlines that carry it into the waste channel. Because the droplets are introduced at 5 kHz, selective and accurate sorting requires that the electrodes be switched on and off well above these rates. Indeed, this can also be accomplished with salt water electrodes, which can dielectrophoretically sort droplets at several kilohertz for hours continuously, as depicted in Fig. 3d.

One last concern is that over hours or days, both water and salt ions could diffuse from the electrode into the surrounding PDMS and channels. We find that after several days of use, the electrodes and moat continue to function properly. This is likely because the slowly-diffusing ions are effectively locked in the PDMS on short time scales and unable to respond to applied fields. If dried and stored, a device can be reused simply by reintroducing a lower concentration solution into the electrode to dissolve residual salt.

Conclusions

We have shown that salt water electrodes are excellent substitutes for metal electrodes for most droplet-based microfluidic operations that require electric fields, including droplet merger, picoinjection, and ultrahigh-throughput sorting. Based on simulations and calculations, we determine this to be the result of the microfluidic channels having small capacitances, permitting signal transmission even in solutions that have poor conductivity relative to metal electrodes. Compared to metal electrodes, salt water electrodes are easier to implement and more robust in operation, as any air gap can be immediately absorbed by the PDMS walls or flushed out. Salt water electrodes greatly simplify device fabrication and should be appropriate for most droplet-based microfluidic workflows.

Acknowledgements

We would like to thank John Haliburton for the design and fabrication of the syringe clamps. This work was supported by an NSF CAREER Award (DBI-1253293), a grant from the NIH (HG007233-01), a Research Award from the California Institute for Quantitative Biosciences (QB3), the Bridging the Gap Award from the Rogers Family Foundation, a New Frontiers Research Award from the UCSF/Sandler Foundation Program for Breakthrough Biomedical Research, and a grant from the University of California Proof of Concept Program.

Notes and references

[a] *Department of Bioengineering and Therapeutic Sciences, California Institute for Quantitative Biosciences, University of California, San Francisco, California, USA. *E-mail: adam.abate@ucsf.edu*

1 S.-Y. Teh, R. Lin, L.-H. Hung, and A. P. Lee, *Lab Chip*, 2008, **8**, 198–220.
2 M. T. Guo, A. Rotem, J. a Heyman, and D. a Weitz, *Lab Chip*, 2012, **12**, 2146–55.
3 R. Seemann, M. Brinkmann, T. Pfohl, and S. Herminghaus, *Rep. Prog. Phys.*, 2012, **75**, 016601.
4 C. Priest, S. Herminghaus, and R. Seemann, *Appl. Phys. Lett.*, 2006, **89**, 134101.
5 K. Ahn, J. Agresti, H. Chong, M. Marquez, and D. a. Weitz, *Appl. Phys. Lett.*, 2006, **88**, 264105.
6 E. Brouzes, M. Medkova, N. Savenelli, D. Marran, M. Twardowski, J. B. Hutchison, J. M. Rothberg, D. R. Link, N. Perrimon, and M. L. Samuels, *Proc. Natl. Acad. Sci. U. S. A.*, 2009, **106**, 14195–200.
7 L. Mazutis, J.-C. Baret, P. Treacy, Y. Skhiri, A. F. Araghi, M. Ryckelynck, V. Taly, and A. D. Griffiths, *Lab Chip*, 2009, **9**, 2902–8.
8 A. R. Abate, T. Hung, P. Mary, J. J. Agresti, and D. a Weitz, *Proc. Natl. Acad. Sci. U. S. A.*, 2010, **107**, 19163–6.
9 L. Mazutis, J. Gilbert, W. L. Ung, D. a Weitz, A. D. Griffiths, and J. a Heyman, *Nat. Protoc.*, 2013, **8**, 870–891.
10 B. El Debs, R. Utharala, I. V. Balyasnikova, A. D. Griffiths, and C. A. Merten, *Proc. Natl. Acad. Sci.*, 2012, **109**, 11570–11575.
11 J. J. Agresti, E. Antipov, A. R. Abate, H. Ahn, A. C. Rowat, J.-C. Baret, M. Marquez, A. M. Klibanov, A. D. Griffiths, and D. A. Weitz, *Proc. Natl. Acad. Sci.*, 2010, **107**, 4004–4009.
12 J.-C. Baret, O. J. Miller, V. Taly, M. Ryckelynck, A. El-Harrak, L. Frenz, C. Rick, M. L. Samuels, J. B. Hutchison, J. J. Agresti, D. R. Link, D. a Weitz, and A. D. Griffiths, *Lab Chip*, 2009, **9**, 1850–8.
13 A. Fallah-Araghi, J.-C. Baret, M. Ryckelynck, and A. D. Griffiths, *Lab Chip*, 2012, **12**, 882–91.
14 A. C. Siegel, S. S. Shevkoplyas, D. B. Weibel, D. a. Bruzewicz, A. W. Martinez, and G. M. Whitesides, *Angew. Chemie*, 2006, **118**, 7031–7036.
15 K. Churski, P. Korczyk, and P. Garstecki, *Lab Chip*, 2010, **10**, 816–8.
16 D. J. Eastburn, A. Sciambi, and A. R. Abate, *Anal. Chem.*, 2013, **85**, 8016-21.
17 D. J. Eastburn, A. Sciambi, and A. R. Abate, *PLoS One*, 2013, **8**, e62961.
18 B. O'Donovan, D. J. Eastburn, and A. R. Abate, *Lab Chip*, 2012, **12**, 4029–32.
19 N. Hallfors, A. Khan, M. D. Dickey, and A. M. Taylor, *Lab Chip*, 2013, **13**, 522–6.
20 J.-H. So and M. D. Dickey, *Lab Chip*, 2011, **11**, 905–11.
21 T. Merkel, V. Bondar, K. Nagai, B. D. Freeman, and I. Pinnau, *J. Polym. Sci.*, 2000, **38**, 415–434.
22 J. Z. Chen, A. a Darhuber, S. M. Troian, and S. Wagner, *Lab Chip*, 2004, **4**, 473–80.
23 J. D. Jackson, *Am. J. Phys.*, 2000, **68**, 789.
24 A. P. Gerratt and S. Bergbreiter, *J. Micromechanics Microengineering*, 2013, **23**, 067001.
25 A. Sciambi and A. R. Abate, *Biomicrofluidics*, 2013, **7**, 044112.